POLITECNICO DI TORINO
Repository ISTITUZIONALE

Paired electrosynthesis of formic acid by CO2 reduction and methanol oxidation. Effect of the anode nature and supporting electrolyte

Original
Paired electrosynthesis of formic acid by CO2 reduction and methanol oxidation. Effect of the anode nature and supporting electrolyte / Meli, P., Antonello, A., Di Franco, A., Galia, A., Greco, L., Ahmed Isse, A., Proietto, F., Scialdone, O.. - In: JPHYS ENERGY. - ISSN 2515-7655. - 8:3(2026), pp. 1-19. [10.1088/2515-7655/ae5e0a]

Availability:
This version is available at: 11583/3012829 since: 2026-07-09T10:33:05Z

Publisher:
Institute of Physics - IOP

Published
DOI:10.1088/2515-7655/ae5e0a

Terms of use:

This article is made available under terms and conditions as specified in the corresponding bibliographic description in the repository

Publisher copyright

(Article begins on next page)

26 November 2026

JPhys Energy

PURPOSE-LED PUBLISHING™

PAPER • OPEN ACCESS

Paired electrosynthesis of formic acid by CO_2 reduction and methanol oxidation. Effect of the anode nature and supporting electrolyte

To cite this article: Paola Meli *et al* 2026 *J. Phys. Energy* **8** 035001

View the article online for updates and enhancements.

You may also like

- (Invited) Formic Acid and Formate Production through Electrochemical Reduction of CO_2 - An Assessment of Technology and Challenges
A. S. Agarwal, S Guan, Y. Zhai et al.

- *(Invited)* Development of Energy-Efficient and Scalable Electrochemical Devices for CO_2 to Formate Conversion
Leiming Hu, Fry Intia, Jacob A Wrubel et al.

- CO_2 Conversion to Formic Acid in a Three Compartment Cell with Sustainion™ Membranes
Hongzhou Yang, Jerry J. Kaczur, Syed D. Sajjad et al.



This content was downloaded from IP address 176.200.25.39 on 08/07/2026 at 12:49

Journal of Physics: Energy

Check for updates

OPEN ACCESS

RECEIVED
19 January 2026

REVISED
17 March 2026

ACCEPTED FOR PUBLICATION
10 April 2026

PUBLISHED
1 July 2026

Original content from this work may be used under the terms of the Creative Commons Attribution 4.0 licence.

Any further distribution of this work must maintain attribution to the author(s) and the title of the work, journal citation and DOI.

PAPER

Paired electrosynthesis of formic acid by CO_2 reduction and methanol oxidation. Effect of the anode nature and supporting electrolyte

Paola Meli[1,3], Andrea Antonello[2], Andrea Di Franco[1], Alessandro Galia[1], Lucrezia Greco[1], Abdirisak Ahmed Isse[2,*], Federica Proietto[1] and Onofrio Scialdone[1,*]

[1] Dipartimento di Ingegneria, Università degli Studi di Palermo, Palermo, Italy
[2] Dipartimento di Scienze Chimiche, Università degli Studi di Padova, Padova, Italy
[3] Department of Applied Science and Technology (DISAT), Politecnico di Torino, Torino, Italy
[*] Authors to whom any correspondence should be addressed.

E-mail: abdirisak.ahmedisse@unipd.it and onofrio.scialdone@unipa.it

Keywords: paired synthesis, CO_2 cathodic reduction, methanol anodic oxidation, formic acid/formate, BDD, $Ni(OH)_2$

Supplementary material for this article is available online

Abstract

The paired synthesis of formic acid/formate (FA) by cathodic reduction of CO_2 and anodic oxidation of methanol was evaluated using aqueous solutions with different supporting electrolytes (SE) (Na_2SO_4, $KHCO_3$, NaOH) and a Sn cathode combined with various anodic materials (Pt, Cu, $Ni(OH)_2$, Ni NPs, $Ti/IrO_2–Ta_2O_5$, Ti/RuO_2, boron-doped diamond (BDD) and Ti_4O_7) with the main aims to evaluate what electrolytes are required by the cathodic and anodic processes and the performances of various anodes in different electrolytes. It was found that the cathodic and anodic processes require very different electrolytes: the cathodic reduction of CO_2 is strongly affected by the adopted SE, and it is favoured by working in acidic solutions. Conversely, methanol oxidation to FA at the anode is favoured by using NaOH solutions at very high pH. Hence, the best results were achieved using different electrolytes in the anodic and cathodic compartments. Ni-based anodes gave the highest faradaic efficiencies (FE_{FA} = 94%–100%) for the FA production in 0.5 M NaOH solutions, especially at low current densities. Just slightly lower FE_{FA} were found under these conditions at BDD anode; moreover, the BDD gave the best results in the other tested electrolytes, although FE_{FA} was significantly lower than in NaOH solutions.

1. Introduction

The electrochemical reduction of CO_2 ($ERCO_2$) has attracted a considerable and increasing attention in the recent years. As an example, the number of manuscripts focused each year on this topic increased by about ten times from 2013 to 2023. Indeed, $ERCO_2$ could be a very attractive alternative for many industries to reduce CO_2 emission into the atmosphere, as they would achieve both lower carbon taxes and higher revenues by selling the higher value-added chemicals produced [1–3]. $ERCO_2$ can be used to produce value-added chemicals, such as carbon monoxide, formic acid and formate (FA), methanol, methane and ethene and higher hydrocarbons [2]. Among these products, up to now, CO and FA are considered among the most interesting ones due to their relatively high market price, the low number of electrons (i.e. 2) necessary to obtain them from CO_2, and the interesting figures of merit reported in the literature [1–4]. However, according to the literature, it is still necessary to improve the process from an economic point of view to develop it on an applicative scale [3–5]. It would be essential to obtain high faradaic efficiencies (FEs) coupled with high productivity of the target product, as well as high stability and relatively low capital and operating costs. Moreover, a proper selection of the anodic process is of paramount relevance to drastically improve the economic perspectives of $ERCO_2$ [5–9]. In most cases, CO_2 reduction is coupled with water oxidation at the anode, which is characterized by a high standard potential of E^o = 1.23 V vs SHE, a high overpotential and by the production of oxygen, which has

© 2026 The Author(s). Published by IOP Publishing Ltd

a relatively low economic value. Replacing this oxidation reaction with a more valuable reaction, in a process called paired electrolysis, can improve the economic figures of the process. Indeed, paired electrolysis can potentially increase the cell's production capacity and reduce its energy requirements. As an example, some of the authors have shown that the adoption of a paired process involving the cathodic reduction of CO_2 to FA and the anodic treatment of liquid effluents contaminated by organic pollutants significantly improves the economic perspectives of both routes [9]. Various other examples of paired $ERCO_2$ processes have been proposed [10] including the oxidation of biomass to formate [11, 12], the conversion of biomass-derived 5-hydroxymethylfurfural (HMF) to 2,5-furandicarboxylic acid [13], the oxidation of urea, alcohols and formaldehyde [14–16] and chlorine evolution [14, 17]. However, even though very promising results have been reported in the literature for some paired electrolysis involving CO_2 conversion to FA, these processes in some cases still require a drastic improvement to achieve a set of operative conditions that allow to optimize both cathodic and anodic processes to obtain an overall route that is economically competitive with conventional ones.

A promising alternative to the oxygen evolution reaction (OER) to be coupled with $ERCO_2$ is the methanol oxidation reaction (MOR) to formate [18]. Indeed, MOR, characterized by a standard potential of +0.016 V vs SHE, requires significantly less energy than OER and enables the production of a higher added value chemical. Noticeably, the average market value of formic acid in the last years was 0.97 \$/kg (44.60 \$/kmol) to be compared with that of methanol, which is valued at 0.46 \$/kg (14.75 \$/kmol) [18, 19]. Formic acid and formate salts are largely used in plastics, agriculture, textiles, and pharmaceutical industries [20] but their conventional synthesis involves multiple steps under harsh conditions [21]. Moreover, the use of suitable anodes, such as Pt, and cathodes, such as Sn or Bi, allows to produce FA, by both MOR (equation (1) or (2) depending on pH) and $ERCO_2$ (equation (3) for acidic pH). The produced FA will be present in the form of acid and/or conjugate base (formate), depending on the pH (equation (4)).

Anode reactions:

$$CH_3OH + 5OH^- \rightleftarrows HCOO^- + 4H_2O + 4e^- \quad (1)$$

$$CH_3OH + H_2O \rightleftarrows HCOOH + 4H^+ + 4e^- \quad (2)$$

Cathode reactions:

$$CO_2 + 2H^+ + 2e^- \rightleftarrows HCOOH \quad (3)$$

$$HCOOH \rightleftarrows HCOO^- + H^+ \, (pK_a = 3.74) \quad (4)$$

Notably, good FEs were obtained using various electrodes such as copper oxide [18, 19, 22], AuIn [12] and nickel-based [16, 23, 24] anodes working at potentials lower than those typically involved in OER. Very promising studies have been focused on this paired process showing its relevant potential interest [17, 20, 22]. However, a quite limited analysis of the effect of operative parameters (such as the nature and the concentration of the supporting electrolyte (SE), the pH, the current density, etc) was usually reported. To develop this paired process, it would be necessary to evaluate what electrolytes are required by both the cathodic and the anodic processes and the effect of the nature of the anode in SEs with different chemical compositions.

This study examines the ($ERCO_2$ + MOR) configuration using a series of anode materials (Ni-based electrodes, boron doped diamond (BDD), Ti_4O_7, Ir and Ru oxides, Pt and Cu) and various electrolytes and pH to determine how both the electrode nature and the SE affect system behaviour. Tin was chosen as a catalytic electrode for the cathodic process. Indeed, Sn has good catalytic properties for $ERCO_2$ and is highly selective for formic acid formation. For these reasons $ERCO_2$ on Sn-based electrodes has been widely investigated and several papers dedicated to the reaction mechanism are available in the literature [25–28].

2. Experimental section

2.1. Materials

Commercially available chemicals, potassium bicarbonate ($KHCO_3$, Sigma Aldrich, 99.7%), sodium hydroxide (NaOH, Sigma Aldrich, ⩾98%), sodium sulphate (Na_2SO_4, Carlo Erba, > 99%), sulfuric

acid (H_2SO_4, Sigma Aldrich, 98%), formic acid (HCOOH, Thermoscientific, 99%), sodium tetrahydroborate ($NaBH_4$, Sigma Aldrich, 99%), isopropanol (iPrOH, Sigma Aldrich, 99.9%), dimethylformamide (DMF, Sigma Aldrich, 99.8%), methanol (CH_3OH, Carlo Erba, High-performance liquid chromatography (HPLC) plus), Nickel(II) sulphate hexahydrate ($NiSO_4.6H_2O$, Sigma Aldrich, 99.5%), Polyvinylpyrrolidone, PVP K30 (Sigma Aldrich), cetyl trimethylammonium bromide ($(C_{16}H_{33})N(CH_3)_3]Br$, Sigma Aldrich, >98%), Nafion binder (Sigma Aldrich, 5 wt% in a mixture of lower aliphatic alcohols and water), mesoporous carbon Vulcan XC72 (Sigma Aldrich) and Nafion® 324 (Sigma Aldrich) were used as received. High purity helium (99.999%) and CO_2 (99.999%) were supplied by Air Liquide and Rivoira, respectively. The electrodes BDD (Condias, Itzehoe, Germany), Ti_4O_7 (Deqing Chuangzhi Technology Co., Ltd), Ti/RuO_2 (Electrocell AB), Ti/IrO_2–Ta_2O_5 (Electrocell AB), Pt (Sigma Aldrich, 99.9%), Cu (Thermo Fisher Scientific, 99.99%), Sn (Carlo Erba, 99.99%) and carbon paper support (AVCarb 370, FuelCellStore) were purchased, whereas Ni-based electrodes, $Ni(OH)_2$ and Ni NPs, were prepared as described below.

2.2. Preparation and characterization of Ni-based electrodes

β-$Ni(OH)_2$ was synthesized by a microwave–hydrothermal process [29]. 1.822 g (5 mmol) of cetyl trimethylammonium bromide were dissolved by slow agitation in 10 ml of water in a 20 ml glass microwave flask (type G30). Then, 0.80 g of NaOH (0.02 mol) and 2.91 g of $NiSO_4 \cdot 6H_2O$ (0.011 mol) were added under gentle stirring to avoid foam formation. After stirring the solution for 5 min, the flask was sealed with a rubber cap and put in a Multiwave PRO microwave (Anton-Paar). The reaction was performed, under magnetic stirring at 800 rpm, by heating the flask to 150 °C at a rate of 40 °C min^{-1}, followed by 30 min at 150 °C and cooling down to 50 °C in 5 min. After the microwave treatment, the solution was left cooling to room temperature for 30 min. The reaction mixture was then transferred to a falcon container and centrifuged at 2000 rpm to yield a light green precipitate, which was recovered and purified with four more cycles of centrifugation each time rinsing the precipitate with 20 ml of water.

For the synthesis of nickel nanoparticles (Ni NPs), 0.40 g of PVP K30 were dissolved in 40 ml of water in a 250 ml two-necked round-bottom flask. After stirring for 15 min and heating to 80 °C, 0.536 g (3.4 mmol) of $NiSO_4 \cdot 6H_2O$ were added to the mixture. In another flask, 1 equivalent of $NaBH_4$ (0.127 g, 3.4 mmol) was dissolved in 50 mL of water. This solution was then added dropwise to the nickel salt solution for a total time of 1 h. The mixture was stirred for 3 additional hours and then left to rest at room temperature for 24 h. The Ni NPs were separated by centrifugation. They were then purified by 3 cycles of centrifugation, each time dispersing the solid in water, followed by precipitation by acetone addition.

All Ni-based electrodes were prepared by spray coating or drop coating catalyst inks, composed of $Ni(OH)_2$ nanosheets or Ni NPs, mesoporous carbon Vulcan XC72 and Nafion binder, on a carbon paper support or glassy carbon (GC). The effective catalyst loading on carbon paper electrodes was determined by weighing the carbon support before and after ink deposition. In the case of $Ni(OH)_2$ electrodes, the ink mixture was 45% $Ni(OH)_2$, 45% Vulcan XC72 and 10% binder, and was prepared by dispersing appropriate amounts of the components in 5 ml of iPrOH/H_2O (80/20, v/v) to obtain a total concentration of 2.5 mg ml^{-1}. The ink was sonicated for 30 min to ensure good dispersion of the components. To prepare electrodes for electrolysis, the ink was transferred to a manual airbrush and spray coated on a 16 cm^2 carbon paper support AVCarb 370, which was held on a hot plate at 100 °C to facilitate solvent evaporation. The catalyst-coated support was then transferred to a petri dish and further dried under vacuum overnight. Electrodes for voltammetric studies were prepared by drop casting 12 μl of an ink of the same composition as the previous one but in DMF/H_2O (80/20, v/v) onto a 3 mm diameter GC disk. The deposited ink was dried at 50 °C for at least 2 h before using the electrode. The total solid component concentration in the ink was 20.0 mg ml^{-1}, which corresponds to a catalyst loading of 0.5 mg cm^{-2} in the electrode.

The ink used for the fabrication of electrodes based on Ni NPs was prepared by dispersing via sonication for 30 min 20.8 mg of a mixture of Ni NPs and Vulcan XC72 (55.6/44.4, w/w) together with 4.2 mg of Nafion binder in 10.0 ml of DMF/iPrOH (30/70, v/v). The total concentration of the solid components in the ink was 2.5 mg ml^{-1}. 4.0 ml of ink was loaded in an airbrush and spray coated on 7.2 cm^2 carbon paper support AVCarb 370 and dried as previously described. This resulted in electrodes with 0.47–0.66 mg cm^{-2} catalyst loading.

The morphology and activity of the prepared electrodes were characterized by scanning electron microscopy, energy dispersive x-ray spectroscopy, x-ray diffraction, tunnelling electron microscopy, and cyclic voltammetry (CV) in different SE.

2.3. Instrumentation

Paired electrolysis experiments were carried out using an Amel potentiostat/galvanostat, model 2549, whereas an Autolab PGSTAT12 potentiostat/galvanostat, equipped with NOVA software (Metrohm AG, The Netherlands) was used for CV in an undivided glass cell equipped with a Pt counter electrode, a saturated calomel reference electrode (SCE) and Ni-based working electrodes.

HPLC, an Agilent 1260 system equipped with a UV detector, was used for the analysis of liquid phase products, while gas phase products were analysed with an Agilent 7890B gas chromatograph equipped with a thermal conductivity detector, using helium at 1 bar as the carrier gas.

pH measurements were made with a Checker® pH Tester (model HI98103) provided by HANNA®.

Scanning electron microscopy (SEM) images were performed with a Zeiss sigma HD FE-SEM equipped with an INCAx-act PentaFET precision spectrometer (Oxford Instruments) using primary beam acceleration voltages between 10 and 20 kV. XRD measurements were performed on a D8 Advance diffractometer (Bruker) in Bragg Brentano geometry equipped with a Cu x-ray source and 40 kV of acceleration voltage. Phase assignments were done with Diffract .EVA software implemented with the COD database after the kα2 stripping.

Morphological and microstructural characterization of the samples was conducted using transmission electron microscopy (TEM) on a JEOL JEM-F200 microscope. Elemental composition and spatial distribution were analysed using an integrated 100 mm^2 silicon drift detector energy-dispersive x-ray spectrometer (EDX).

2.4. Electrolysis procedure

All electrolysis were carried out in a conventional divided glass cell, using a Sn foil cathode together with one of the following anodes: BDD, Ti_4O_7, Ti/RuO_2, Ti/IrO_2–Ta_2O_5, Pt, Cu, $Ni(OH)_2$ and Ni NPs. The working area of both cathode and anode was 2.4 cm^2. A Nafion® 324 cation exchange membrane, selected for its chemical stability and durability under harsh electrochemical conditions, including the presence of strong acidic and alkaline environments and large pH gradients across the membrane [30], was used to separate the electrode compartments. Each compartment was filled with 75 ml of the same electrolyte solution, except in few cases. Every experiment was independently replicated to confirm the reproducibility of the results, and the corresponding standard deviations are reported in the figures. Before electrolysis, the catholyte was saturated with CO_2 by bubbling the gas for 30 min and CO_2 bubbling was then maintained continuously throughout the entire electrolysis. No CO_2 was added to the anolyte, which instead contained 0.5 M methanol. $KHCO_3$, NaOH and Na_2SO_4 were used as SE. Sulfuric acid was used to acidify the solutions and adjust the initial pH. The experiments were performed without stirring of the solution. Note, however, that mixing was ensured by continuous bubbling of CO_2 during electrolysis.

The temperature was kept constant at 20 °C. A constant current density j (from 11 to 33 mA cm^{-2}), based on the geometric area of the tin foil cathode, was applied for 2 h during which samples for HPLC analyses were periodically withdrawn with a syringe. Before each experiment, all electrodes were sonicated in HPLC-grade water for 5 min and then rinsed with the same solvent. Due to the spontaneous formation of a native oxide layer upon air exposure, the Sn electrode was mechanically polished with sandpaper with varying grit sizes, washed with HPLC-grade water and sonicated. Also, the nickel-based electrodes were activated by 50 voltammetric scans between 0 V and 0.7 V vs SCE at a scan rate of 0.1 V s^{-1}. Blank tests were performed in the absence of current in the presence of 2 mM FA only in the catholyte or in the anolyte, respectively, for 2 h with the same cell used for the electrolysis using aqueous solutions of 0.1 M Na_2SO_4 in the cathodic compartment and 0.5 M NaOH and 0.5 M CH_3OH in the anodic one. No cross-over of formate was observed in both cases. Moreover, the pH in the two compartments did not change appreciably with the time.

2.5. Analysis methods and performances

The concentration of formic acid/formate (FA) in solution was determined by HPLC using a Rezex ROA-Organic Acid H+ (8%) column at a constant temperature of 20 °C. Detection was carried out using a UV detector set at 210 nm, with a 0.005 N aqueous H_2SO_4 solution (pH 2.5) as the mobile phase, flowing at 0.5 mL min^{-1}. Under these conditions, FA showed a retention time of 18.5 min. Formic acid calibration curves were obtained by preparing standard solutions from pure formic acid in the concentration range of 0.1–50 mM. A linear response was observed over the entire range, with a correlation coefficient (R^2) of 0.9999.

The quantity of gaseous products in the anodic compartment, specifically CO and CO_2, was determined by gas chromatography using a Supelco Carboxen® 60/80 column with a temperature program consisting of three steps: first, the temperature was maintained at 35 °C for 5 min, then it was increased to

225 °C at a rate of 20 °C per minute, and kept constant for 8 min. For each injection, a Hamilton syringe GasTight with a volume of 50 μL was used. Finally, the total organic carbon (TOC) was analysed by a TOC-L CSH/CSN Shimadzu analyser.

The performance of the process was evaluated by calculating:

- Faradaic efficiency of the products

$$FE_{FA} = [n \cdot F \cdot V \cdot [FA] / (I \cdot t)] \cdot 100 \quad (5)$$

$$FE_{CO} = [n \cdot F \cdot V \cdot [CO] / (I \cdot t)] \cdot 100 \quad (6)$$

$$FE_{CO_2} = [n \cdot F \cdot V \cdot [CO_2] / (I \cdot t)] \cdot 100 \quad (7)$$

where n is the number of electrons exchanged (2 for $ERCO_2$ to FA, 4 for MOR to FA or CO, and 6 for MOR to CO_2), F is the Faraday constant (96485 C mol^{-1}), V (L) refers to the volume of the liquid solution for liquid products (75 mL) and the headspace volume for gaseous products (37 mL), [FA], [CO] and [CO_2] are the concentrations (mol L^{-1}) of FA, CO and CO_2 respectively.

TOC analysis was performed in the anode compartment to verify that methanol oxidation did not proceed toward complete mineralization to CO_2, but rather toward the formation of liquid products.

$$X_{TOC} = \left([TOC]^0 - [TOC]^f\right) / [TOC]^0 \quad (8)$$

where $[TOC]^0$ and $[TOC]^f$ are the TOC concentrations before and after the electrolysis.

3. Results and discussion

3.1. Characterization of Ni-based electrodes

X-ray diffraction patterns of $Ni(OH)_2$ nanosheets and Ni NPs are reported in figure 1. The prominent peaks observed for $Ni(OH)_2$ are those of β-$Ni(OH)_2$ and are assigned to the (100), (101), (102), (110), (111), and (200) lattice faces [29]. The diffractogram confirmed the purity of the $Ni(OH)_2$ catalyst and showed a preferential growth of the material along the 100 plane. Crystalline size along the direction identified by this plane, determined with the Scherrer equation as described in SI, was found to be 17.9 nm (table S1).The Ni NPs showed broad peaks falling in the region of the main peaks of metallic Ni and β-$Ni(OH)_2$ lattice faces. The presence of the hydroxide is due to Ni oxidation during the purification steps that were carried out in the atmosphere after the synthesis of the NPs [31].

TEM analysis of Ni NPs allowed determination of nanoparticles distribution with a mean diameter of approximately 18 nm (figure S1). TEM images confirm the presence of a core-shell structure formed after catalyst purification as evidenced by a clear contrast between the inner part of the nanoparticle and its outer shell (figures S2 and S3). Different phases were identified by small angle electron diffraction and STEM-EDX analysis (figures S4 and S5) as described in the SI. This analysis provided compelling evidence for the core-shell structure of the Ni NPs, where the core consists of Ni/NiO and the shell is composed of β-$Ni(OH)_2$ sheets and amorphous $Ni(OH)_2$.

SEM images and EDX elemental maps of $Ni(OH)_2$ and Ni NPs electrodes are presented in figure 2. Backscattered electron imaging reveals the presence of micrometric aggregates, identified as brighter regions enriched in Ni, particularly prominent in the $Ni(OH)_2$ sample (figures 2 (c) and (d)).

In contrast, aggregates of Ni NPs are more readily disrupted during ink sonication, resulting in a more uniform dispersion of the material. Notably, inhomogeneous ink distribution during the air-brushing deposition process is excluded, given the homogeneous fluorine signal originating from the binder atoms and the consistent dispersion of the active material across the carbon paper substrate (figures 2 (e) and (f)).

The electrocatalytic activity of $Ni(OH)_2$ and Ni NPs supported on 3 mm diameter GC disks was investigated by CV in NaOH. It has been previously shown that Ni-based electrodes are activated by consecutive cyclic sweeps in an alkaline medium [32]. Examples of CV curves recorded in 0.5 M NaOH are reported in figure 3(A) and figure S6. In 0.5 M NaOH without added methanol, both electrodes exhibit, after activation, an oxidation peak at 0.46 V followed by an intense oxidation current at $E > 0.55$ V vs SCE, which is attributed to OER. In the reverse scan a cathodic peak is observed at 0.22 V vs SCE. This peak is associated with the anodic one at 0.46 V vs SCE as it is observed even if

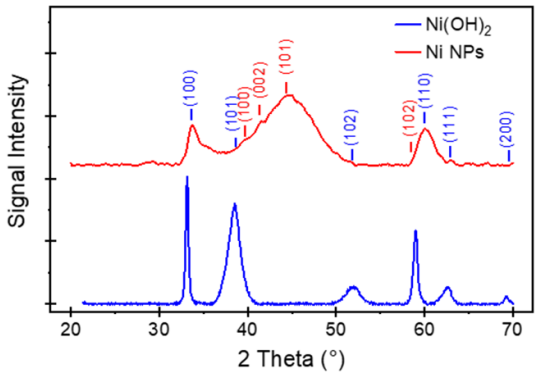


Figure 1. XRD of $Ni(OH)_2$ nanosheets prepared with the microwave procedure and Ni NPs prepared with the wet synthetic method. Characteristic peak positions for $Ni(OH)_2$ (blue) and metallic Ni (red) phases are also reported.

the anodic scan is reversed before the onset of OER. Thus, in agreement with the literature [32–35], the peak couple is assigned to the reversible oxidation of $Ni(OH)_2$ to nickel oxyhydroxide equation (9).

$$Ni(OH)_2 + OH^- \rightleftarrows NiO(OH) + H_2O + e^- \quad (9)$$

According to equation (9), the rate of $Ni(OH)_2$ oxidation to NiO(OH) is expected to be influenced by [OH] and, indeed, the intensity of the peak couple strongly depends on solution pH (figures 3(B) and S7). As shown by XRD and EDX analyses, Ni NPs already contain surface $Ni(OH)_2$, which is further increased by Ni corrosion when the electrode is exposed to the 0.5 M NaOH solution [36] and by electrooxidation during the initial cycles of activation. Therefore, the activated Ni NPs are covered by a layer of $Ni(OH)_2$ and consequently they behave just like the $Ni(OH)_2$-based electrode.

Addition of MeOH to a 0.5 M NaOH solution results in remarkable changes of the CV pattern on both electrode materials (figures 3(C) and S8). A new oxidation peak, partially overlapping the anodic peak of $Ni(OH)_2$, appears as a shoulder of the OER current and increases with increasing MeOH concentration while the cathodic peak at ca 0.22 V vs SCE in the reverse scan decreases, almost disappearing at [MeOH] = 1.0 M. This new process is MeOH oxidation. The electrocatalytic oxidation of methanol on Ni-based catalysts has been widely investigated and there is general agreement in the literature that a prerequisite of the catalytic process is the presence of surface $Ni(OH)_2$ which is oxidized to NiO(OH) (equation (9)) [24, 37–41]. Indeed, the transient formation of NiO(OH) during MOR on nickel-based electrodes has been shown by using spectroelectrochemical techniques [39, 40].

Electrochemical active surface area (ECSA) measurements, conducted under identical mass loadings (as detailed in the SI), revealed a fivefold higher mass activity for Ni NPs (62.7 $m^2\ g^{-1}$) than $Ni(OH)_2$ nanosheets (13.1 $m^2\ g^{-1}$). The enhanced mass activity of the Ni NPs can be attributed to both the higher availability of active Ni sites in the less compact amorphous structure and the overall improved dispersion of the catalytic material on the carbonaceous support shown by EDX (figure 2). However, when normalized by ECSA, the $Ni(OH)_2$ catalyst demonstrated superior site-specific activity, as evidenced by the higher catalytic current it exhibited in comparison with Ni NPs (figure 3(d)). This suggests that higher site activity arises from the crystalline material active phase over the amorphous one.

3.2. Effect of the nature of the anode in NaOH solutions

Pt-, Pd- and Rh-based anodes are among the most active catalysts for MOR [42, 43]. These materials present various drawbacks including the tendency to oxidize MeOH to CO_2, high cost and potential CO poisoning [42, 43]. Among the non-noble metals, Ni-based anodes are often used, followed by Co, Fe, Mo, and Cu [42]. Formate production via MOR was widely investigated at high pH, since basic conditions with high [OH^-] favour MeOH oxidation at various electrodes [44]. However, neutral or acidic pH are largely used to favour CO_2 reduction to FA at various cathodes, including Sn [6]. Hence, we decided to evaluate the effect of the anode material using a Sn foil cathode and different SEs. Various anodes were used, including:

- Pt-, Ni- and Cu- based electrodes which are among the most studied anodes for the MOR and were reported to be able to oxidize MeOH to formate [22, 23, 37, 42, 45];

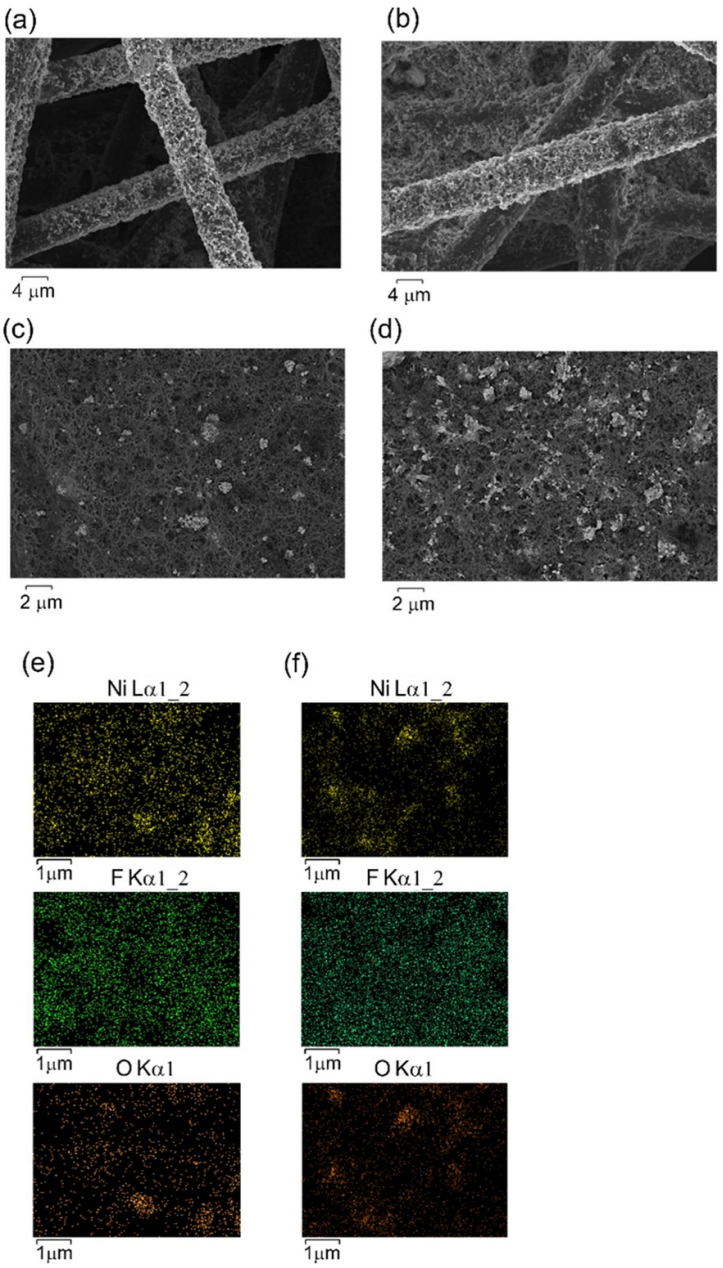


Figure 2. SEM images and EDX elemental maps of carbon paper supported electrodes of Ni NPs (0.40 mg cm^{-2} of catalyst loading) (a, c, e) and $Ni(OH)_2$ (0.53 mg cm^{-2} of catalyst loading) (b, d, f). (a, b) Backscattered electron images showing the surface morphology of the electrodes at an acceleration voltage of 5.0 kV; (c, d) secondary electron images illustrating the distribution of aggregates on the electrode surfaces; (e, f) EDX maps depicting the elemental distribution of Ni (yellow), F (green), and O (orange).

- $Ti/IrO_2–Ta_2O_5$ and Ti/RuO_2 which are known to present a relatively low oxygen overpotential, enabling selective oxidation of organics at room temperature [46], and are largely used in industry for oxygen and chlorine evolution, respectively;
- BDD which exhibits a markedly high oxygen overpotential, thus allowing electro oxidation of many organics, including CH_3OH to FA, even up to their mineralization [46];
- Ti_4O_7 which in many cases presented intermediate results between Ir or Ru oxides and BDD [47].

A first set of experiments was performed for 2 h in a divided cell using a Sn cathode and different anodes. The tests were conducted in a galvanostatic mode with a constant current density of 11 mA cm^{-2}. It must be noted that from here onwards the current density is calculated using the geometric area of the electrodes. ECSA could not be used because of the lack of reliable methods of determination of this parameter for all investigated electrodes. The SE in both compartments was an aqueous

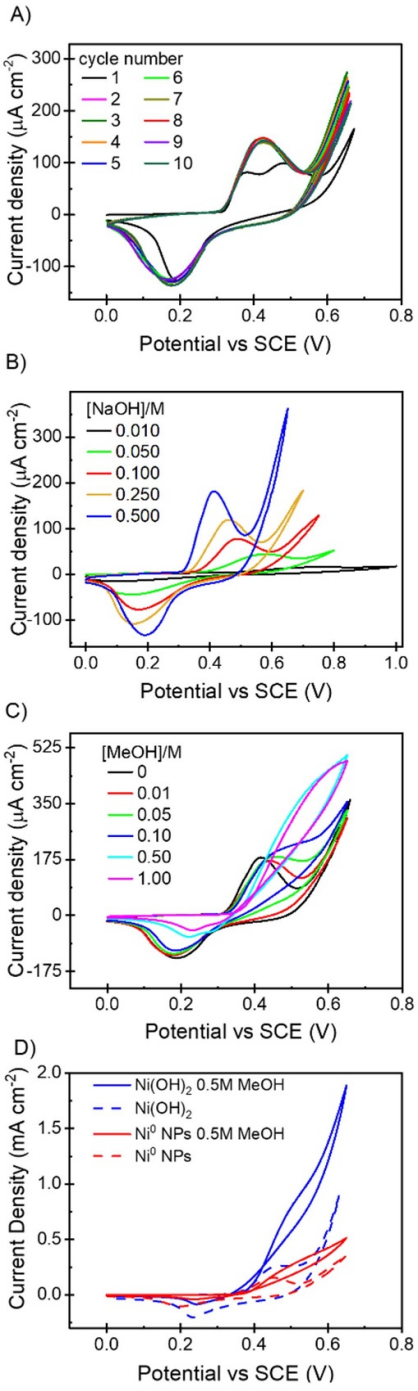


Figure 3. ECSA normalized cyclic voltammograms recorded at 50 mV s^{-1} on Ni NPs and $Ni(OH)_2$ supported on a 3 mm GC disk (0.5 mg cm^{-2}) in alkaline solutions in the absence and presence of MeOH: A) consecutive activation CVs for Ni NPs; B) effect of NaOH concentration, acting also as the background electrolyte, on CV pattern of Ni NPs; C) effect of MeOH concentration on CV pattern of Ni NPs in 0.5 M NaOH; D) comparison between Ni NPs (red) and $Ni(OH)_2$ catalysts (blue) in 0.5 M NaOH with and without MeOH (0.5 M).

solution of 0.5 M NaOH. This OH^- concentration was chosen on the basis of a preliminary assessment of the effect of the hydroxide ion on the performance of Ni NPs anodes for MeOH oxidation to formic acid/formate (see supporting information).

Methanol (0.5 M) was added to the anolyte while the catholyte was fed with CO_2.

Figure 4(A) reports the evolution of the concentration of FA in the anolyte during the electrolysis for the different anodes tested. The Pt anode gave a significant production of FA in the anolyte with a final concentration after 2 h close to 3.6 mM and a FE_{FA} close to 50% (figure 4(B)). According to the literature, the use of Pt allows the production of FA with FE_{FA} close to 100% at quite low potentials and small current densities (<0.01 mA cm^{-2}) [48]. However, when the working potentials and the initial current densities were increased, a significant reduction of FE_{FA} was observed, which, according to in-

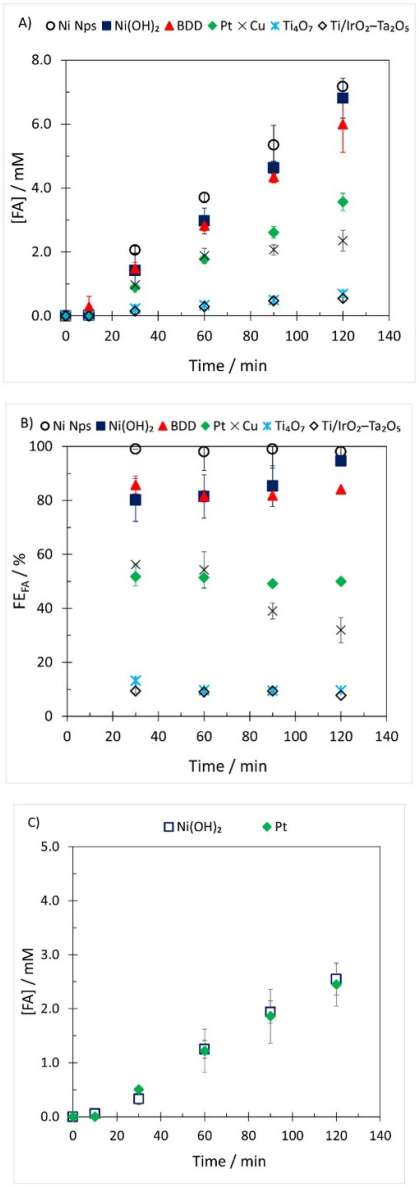


Figure 4. Paired CO_2/methanol electrolysis performed at 11 mA cm^{-2} for 2 h using a Sn cathode and different anodes in a divided cell with an aqueous solution of 0.5 M NaOH in both compartments and 0.5 M CH_3OH in the anolyte. Effect of the nature of the anode on FA production (A) and FE_{FA} (B) in the anodic compartment, and FA production (C) in the cathodic compartment for experiments performed with Pt and $Ni(OH)_2$ anodes.

situ FTIR studies, was presumably caused by the partial oxidation of formate to CO_2 and adsorbed CO [48, 49]. When the Pt anode was replaced with Cu-, Ir- and Ti-based anodes, a lower production of FA was observed (figure 4(A)). In particular, $Ti/IrO_2–Ta_2O_5$ gave the lowest FE_{FA} close to 7%. These results are coherent with the fact that this anode is characterized by a low overpotential for oxygen evolution, thus favouring anodic oxidation of water with respect to organics oxidation [45]. The anodic oxidation of water involves the formation of hydroxyl radicals, which can be either physically or chemically adsorbed on the anode surface. In the case of IrO_2- or RuO_2- based anodes, hydroxyl radicals strongly interact with the electrode surface, forming higher oxides or super oxides, which evolve easily towards the oxygen evolution [45]. The Ti_4O_7 anode gave quite similar and constant FE_{FA} close to 10%. In the case of Cu, a quite different scenario was observed. Indeed, in this case, a relatively high initial FE_{FA} was observed (close to 60%) which decreased over time (figure 4(B)), coherently with the low stability reported in the literature for these anodes.

Conversely, when BDD or Ni-based anodes were used, significantly higher concentrations of FA were produced. Indeed, for these anodes, a final concentration of FA higher than 6 mM was obtained after 2 h (figure 4(A)) with final FE_{FA} values of approximately 100%, 89% and 85% for Ni NPs, $Ni(OH)_2$ and BDD, respectively. Ni-based electrodes have already shown good performance for MOR to FA

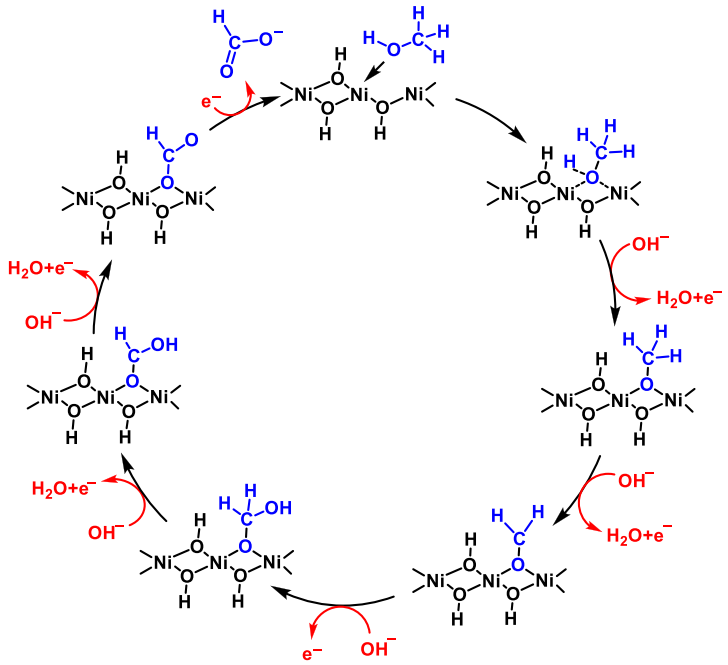


Figure 5. Possible mechanism of MOR to formate based on oxygen vacancies as active sites [24]. Adapted with permission from reference [24]. Copyright 2024 American Chemical Society.

[23, 37, 39] and the results obtained in this study with Ni NPs and $Ni(OH)_2$ are consistent with the existing literature. Despite similar catalyst loading for the two Ni-based anodes, Ni NPs showed better performance than $Ni(OH)_2$. The superior mass activity of Ni NPs may be due to the enhanced dispersion of the NPs within the active layer, as confirmed by EDX compositional analysis, resulting in enhanced electrochemical active surface area (see supporting Information, figure S9). MOR at Ni-based electrodes proceeds by oxidation of $Ni(OH)_2$, either pre-existing as in $Ni(OH)_2$ catalysts or formed *in-situ* by Ni electro oxidation, to nickel oxyhydroxide (equation (9)), which is considered to be the active species involved in the anodic oxidation of MeOH to formate [24, 37–41].

A detailed mechanistic investigation of MOR on Ni-based electrodes has recently been reported by Burgess and co-workers [24]. They proposed that oxygen vacancies, generated on NiOOH surface after $Ni(OH)_2$ oxidation, act as the active catalytic sites. The presence of O-vacancies has been experimentally evidenced by XPS analysis, whereby a relative ratio of vacant oxygen to lattice oxygen of 51:49 has been found. Based on *in-situ* surface-enhanced infrared absorption spectroscopy and density functional theory calculations, they proposed a mechanism involving initial adsorption of MeOH on the vacant site, followed by a sequence of oxidation/deprotonation steps proceeding through various adsorbed intermediates until adsorbed formic acid, $CH(OH)O^*$, is formed (figure 5). This intermediate is then deprotonated by OH^- to give adsorbed formate, $HCOO^*$, which upon one electron transfer desorbs, regenerating the active O-vacancy site. Other reaction pathways leading to CO_3^{2-} formation, which in our experimental conditions appears negligible, were also proposed at very positive oxidation potentials [24].

BDD was shown to be able to oxidize many organics in many cases up to their mineralization [46]. However, it was shown that the oxidation of many organic molecules, such as phenolic compounds, proceeds at BDD with the formation of carboxylic acids, such as FA and oxalic acid, which are more resistant to the successive oxidation than the starting compounds [50, 51], thus potentially allowing their accumulation in the cell. According to the literature, at BDD, the MeOH oxidation can occur directly at the anode at potentials lower than those required by the OER [52]. However, if the potentials are sufficiently high to activate water oxidation, the production of adsorbed hydroxyl radicals is expected (equation (10)), triggering oxidation of small organic molecules, such as MeOH (equation (11)) [52–54]. Indeed, it is well known from the literature that at sufficiently high anodic potentials BDD generates hydroxyl radicals that can effectively oxidize organic species present in solution [46]. In particular, some of the authors have very recently shown that BDD anodes can be used to convert MeOH to FA [55].

$$BDD + H_2O \rightarrow BDD\,(HO^*) + H^+ + e^- \quad (10)$$

$$BDD(HO^*) + R \rightarrow BDD + RO + H^+ + e^- \quad (11)$$

For BDD and Ni-based anodes, gas chromatography analyses of the gaseous phase showed the presence of small amounts (FE < 1%) of both CO and CO_2, thus suggesting that both partial oxidation of methanol to CO (equation (12)) and full oxidation to CO_2 (equation (13)) are negligible side-reactions at these electrodes under adopted operative conditions. Production of small amounts of oxygen was also detected for $Ni(OH)_2$ and BDD (FE < 10%), while in the case of Ni NPs no O_2 was detected due to the production of FA with FE_{FA} close to 100%.

$$CH_3OH \rightarrow CO + 4H^+ + 4e^- \quad (12)$$

$$CH_3OH + H_2O \rightarrow CO_2 + 6H^+ + 6e^- \quad (13)$$

The cathodic reduction of CO_2 resulted in the production of FA. Hence, it was possible to produce FA in both compartments. However, the final concentrations of FA in the catholyte were quite low in all these experiments and close to 2.5 mM due to the occurrence of relatively low FE_{FA}, lower than 20%. In particular, for all adopted anodes, very similar and low FA productions were achieved in the cathodic compartment as illustrated in figure 4(C) for tests performed with $Ni(OH)_2$ and Pt. Very low FE in CO (<4%) were recorded, while very high FE in H_2 (>70%) were observed. These results were attributed to the very high pH used in this series of experiments.

3.3. Effect of the nature of the anode in $KHCO_3$ and Na_2SO_4 electrolytes

A second series of experiments was performed for 2 h at a current density of 11 mA cm^{-2} in a divided cell containing a 0.1 M aqueous solution of $KHCO_3$ or Na_2SO_4 in both compartments. Tin was used as cathode while various electrode materials were tested as anode. $KHCO_3$ and Na_2SO_4 were chosen since $ERCO_2$ in these electrolytes was previously shown to produce FA with good FEs at various cathodes [54]. MeOH (0.5 M) was added to the anolyte while the catholyte was fed with CO_2.

First experiments were performed in $KHCO_3$ using various anodes (Pt, Cu, $Ti/IrO_2–Ta_2O_5$, Ti/RuO_2, BDD and Ti_4O_7). Ni-based anodes were not used because they showed limited activity at pH < 12. The use of a bicarbonate solution allowed to have a final pH of approximately 7 in both compartments. In good agreement with the literature on $ERCO_2$ at Sn electrocatalysts [6], FA was produced in the cathodic compartment with a relatively high FE_{FA} close to 60% for all experiments.

On the other hand, in the anodic compartment, very different concentrations of FA ([FA]) were achieved depending on the anode used (figure 6(A)). Indeed, Cu, Ti/RuO_2 and Ti_4O_7 gave a very small production of FA ([FA] < 0.2 mM), while much higher [FA] was achieved at BDD, thus confirming the ability of this anode to favour the oxidation of organics at various pH [53]. Intermediate results were obtained with Pt and $Ti/IrO_2–Ta_2O_5$.

This set of experiments shows that BDD behaves better than other anodic materials. It must be noted, however, that the observed FE_{FA} was quite small (slightly lower than 20%), much lower than that observed in alkaline media. The production of other oxidation products was evaluated. Various anodic processes can take place in aqueous solutions of MeOH, such as conversion of the alcohol to CO (equation (12)) and CO_2 (equation (13)) as well as oxygen evolution. Indeed, a FE in CO (FE_{CO}) of approximately of 10% was obtained, whereas the FE in CO_2 (FE_{CO2}) was higher than 50% because of the high mineralization ability of BDD [46]. High mineralization of MeOH coupled with a quite low CO production (FE_{CO} = 4%) was observed also at the Pt anode.

Since various authors have reported that the $ERCO_2$ to FA at Sn can benefit from the utilization of slightly acidic pHs, some tests were performed using Na_2SO_4 as SE with Pt or BDD as anode. In this case, the initial pH was about 4.2 in the cathodic compartment due to the acidification by dissolved CO_2 and 6.5 in the anodic one. After 2 h of electrolysis, the pH in the cathodic compartment slightly increased to values close to 6 because the cathodic processes consume protons, while that of the anodic compartment decreased to about 2 since anodic reactions involve release of H^+ in solution. Also in this case, BDD gave better results than Pt (figure 6(B)), with a FE_{FA} in the anolyte of approximately 35% and 14% for BDD and Pt, respectively.

3.4. Effect of the nature of the SE

Figure 7 and table 1 report the effect of both anode and SE on the performances of the paired process. As shown in figure 7, in the case of the anodic process at both Pt (figure 7(A)) and BDD (figure 7(B)) anodes, the replacement of NaOH, which guarantees a very high pH close to 14, with $KHCO_3$ or

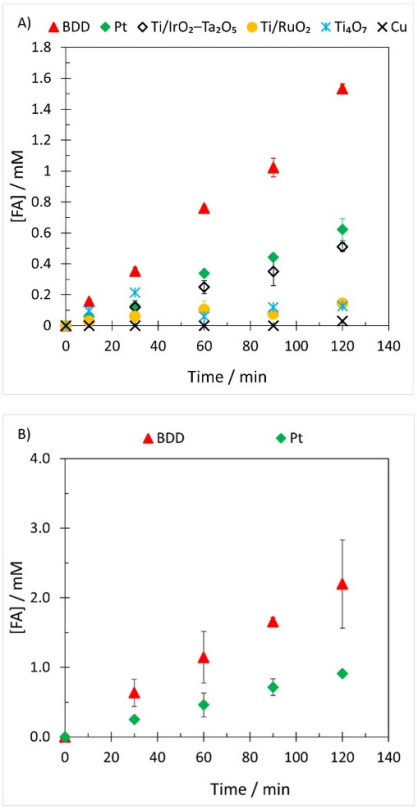


Figure 6. Effect of the nature of the anode on FA production in the anodic compartment of paired CO_2/methanol electrolysis performed at 11 mA cm^{-2} for 2 h, using a Sn cathode in a divided cell with 0.1 M aqueous solutions of $KHCO_3$ (A) or Na_2SO_4 (B) in both compartments and 0.5 M CH_3OH in the anolyte.

Na_2SO_4, which give rise to quasi neutral and acidic conditions, respectively, resulted in a marked reduction of [FA] in the anolyte and of the corresponding FE_{FA} (table 1). For Pt, the final [FA] was 0.7, 0.9 and 3.6 mM using $KHCO_3$, Na_2SO_4 and NaOH, respectively. Similarly, for BDD, the final [FA] was 1.5, 2.3 and 6.0 mM using $KHCO_3$, Na_2SO_4 and NaOH, respectively. Similar results were obtained for all the other tested anodes replacing NaOH with $KHCO_3$ (figures 4(A) and 6(a)). According to the literature, the better performance of Pt achieved in alkaline media as compared to neutral or acidic media is due to various factors including (*i*) the positive effect of high pH and high bulk OH^- concentrations on MeOH oxidation and (*ii*) the detrimental effect of high pH on FA oxidation to CO_2. Indeed, it has been reported that the electro-oxidation of MeOH on Pt requires the presence of OH adsorption, which is favoured at high pH and, hence, high bulk OH^- concentrations [44, 56].

Based on various works in the literature, the electrochemical oxidation of MeOH on Pt follows a dual-path mechanism:

(*i*) an indirect pathway, which involves MeOH dehydrogenation to adsorbed CO, which is subsequently oxidized to CO_2/CO_3^{2-} or (*ii*) a direct pathway leading to the formation of soluble intermediates or products such as formaldehyde (HCHO) and formic acid/formate ($HCOOH/HCOO^-$) [48, 57]. Even though some authors have proposed a different pathway, there is large consensus that pH and OH^- concentration significantly influence the reaction mechanism, thereby altering the FEs of CO_2/CO_3^{2-} and $HCOOH/HCOO^-$ [48].

Moreover, John *et al* [56] have reported that the oxidation of $HCOO^-$ to CO_2 in an alkaline medium occurs to a significantly lower extent compared to HCOOH oxidation in acidic media. Indeed, according to various authors, the oxidation of HCOOH takes place only after being converted to $HCOO^-$ via the acid-base equilibrium and consequently is strongly dependent on pH [57].

Conversely, the opposite electrolyte effect was observed for the cathodic process. In this case, the best performances were achieved using Na_2SO_4, whereas the worst FA production was obtained with NaOH (figure 7(C) and table 1). For example, in the paired electrolyses with Sn cathode and BDD anode, the FE_{FA} of the cathodic process was 18%, 58% and 70% using NaOH, $KHCO_3$ and Na_2SO_4, respectively. Indeed, it has been reported that the cathodic reduction of CO_2 at Sn cathodes benefits from the use of Na_2SO_4 as SE [54]. In particular, the FE_{FA} can be optimized using an acidified aqueous solution of

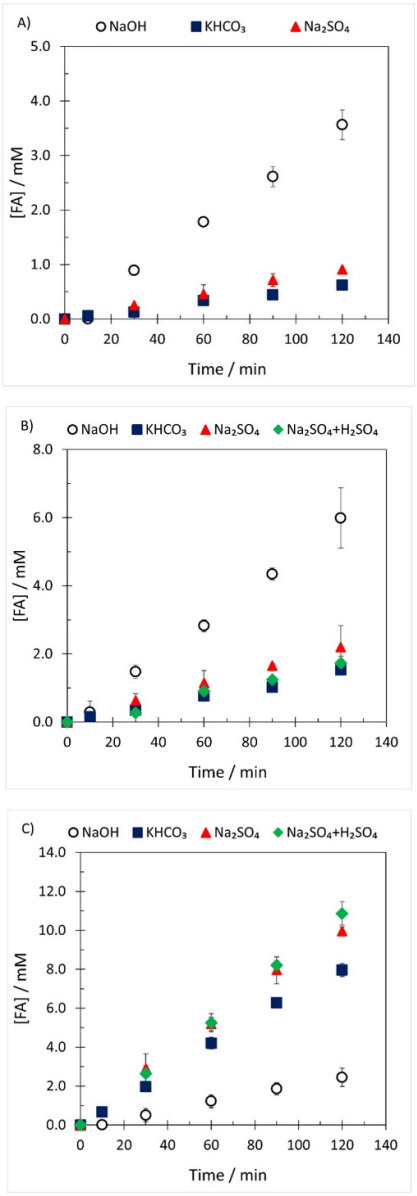


Figure 7. Effect of the supporting electrolyte (0.1 M $KHCO_3$, 0.1 M Na_2SO_4 or 0.5 M NaOH) on FA production in paired CO_2/methanol electrolysis at a Sn cathode and a Pt or BDD anode, performed at 11 mA cm^{-2} for 2 h in a divided cell containing the same electrolyte in both compartments and 0.5 M CH_3OH in the anolyte. FA production in the anodic compartment at Pt (A) and BDD (B) anodes, and in the cathodic compartment (C) when BDD was used as anode.

Na_2SO_4 with an initial pH of approximately 3 [54]. The negative effect of higher pH on the performance of $ERCO_2$ can be related to various effects, especially (*i*) the reduced concentration of CO_2 due to its transformation into HCO_3^- and CO_3^{2-} and (*ii*) the reduced concentration of a good proton donor, such as H_3O^+, necessary for the FA production. Hence, the electrolysis with Na_2SO_4 was repeated by acidifying the electrolyte with H_2SO_4 to fix the initial pH at 3. As shown in figure 7(C) and table 1, the use of an acidified solution allowed to further enhance the production of FA in the cathodic compartment with an increase of FE_{FA} from 70% to 76% (table 1, entries 7 and 8). However, a slight decrease of FE_{FA} for the anodic process from 31% to 29% (table 1, entries 7 and 8) was observed.

The energetic aspects of the process, namely, the average cell potential (ΔV) during electrolysis and the corresponding energy consumption (EC) were evaluated and reported in table S6 in SI. The lowest ECs were observed for the experiments performed with $Ni(OH)_2$ and Ni NPs anodes using NaOH as SE due to the larger overall production of FA and the smaller ΔVs.

3.5. Paired electrolysis with different electrolytes in the anodic and cathodic compartments

Since the cathodic and the anodic processes require, according to the above-mentioned experiments, quite different SEs, a series of experiments was performed using NaOH in the anolyte and Na_2SO_4 in

Table 1. Effect of the anode and SE on the production of FA in paired $ERCO_2$/MOR electrolysis at a Sn cathode.[a]

Entry	Anode	SE[b]	Average pH in the anolyte	Average pH in the catholyte	FE_{FA} cathode (%)	FE_{FA} anode (%)
1	Pt	NaOH	13	11	16 ± 1.5	52 ± 3.8
2		$KHCO_3$	7.5	6.9	62 ± 1.8	9 ± 1.0
3		Na_2SO_4	4.3	5.0	70 ± 2.1	12 ± 0.0
4	$Ni(OH)_2$	NaOH	14	11	18 ± 1.9	89 ± 7.6
5	BDD	NaOH	13	11	18 ± 2.8	85 ± 12.3
6		$KHCO_3$	7.5	7.0	58 ± 0.8	17 ± 0.6
7		Na_2SO_4	4.0	4.9	70 ± 1.6	31 ± 3.5
8	BDD	Na_2SO_4 (+H_2SO_4)[c]	2.7	4.7	76 ± 4.2	29 ± 2.0
9	BDD	Na_2SO_4 (cath.) NaOH (anol.)	13.3	5.0	69 ± 4.4	83 ± 1.5
10	Ni NPs	Na_2SO_4 (cath.) NaOH (anol.)	13.5	5.0	69 ± 4.3	100 ± 8.8

[a]Electrolysis performed in a divided cell at 11 mA cm^{-2} for 2 h at 20 °C. [b] SE concentration: 0.1 M $KHCO_3$ or Na_2SO_4 and 0.5 M NaOH; 0.5 M CH_3OH in the anolyte and CO_2 saturation in the catholyte. [c] 1 M H_2SO_4 added to adjust the initial pH at 3.

the catholyte; the experiments were carried out at 11 mA cm^{-2} using a Sn cathode combined with a BDD or a Ni-based anode. The utilization of different electrolytes in the two compartments allowed to achieve, for experiments performed at BDD anode, relatively high final [FA] in both compartments close to 6 and 10 mM in the anolyte and in the catholyte, respectively, with a corresponding FE_{FA} of 83% and 69% (table 1, entry 9). When the BDD anode was replaced with Ni NPs, the FA yield in the anodic compartment was improved while the cathodic process remained unaffected. Indeed, in this case, the final [FA] at the Ni NPs anode was approximately 7.2 mM with a nearly 100% FE_{FA} (table 1, entry 10).

To evaluate the effect of the current density on the process, a series of tests was performed maintaining the separated two-electrolytes cell set-up; three current density values (j = 11, 22 and 33 mA cm^{-2}) were tested. Figure 8(A) reports the results achieved with the Ni NPs anode. The increase of j from 11 to 22 mA cm^{-2} allowed to increase significantly the production of FA in the anodic compartment for the same time passed and, consequently, the final [FA] (from 7.2 to 13.3 mM) even if with a slight decrease of the FE_{FA} (figure 8(A)) from about 100 to 94%. A further increase of j from 22 to 33 mA cm^{-2} resulted in negligible changes on FA production rate (figure 8(A)) because of a significant decrease of the FE_{FA} when j = 33 mA cm^{-2} was used (figure 8(B)), which presented a final value of approximately 65%. In the case of the cathodic compartment, a worst scenario was observed. Indeed, the increase of j from 11 to 22 mA cm^{-2} gave a very small increase in FA production rate (figure 8(C)), because of a substantial decrease of the FE_{FA} (figure 8(d)) from about 73% to 39%. When j was increased to 33 mA cm^{-2}, the FE_{FA} decreased to values close to 20% with a significant decrease of FA production rate. Indeed, the cathodic reduction of CO_2 at one atmosphere is characterized by relatively low limiting current densities (j_{lim}) (slightly higher than 10 mA cm^{-2}) due to the low solubility of CO_2 in water. Hence, for j higher than 11 mA cm^{-2}, $ERCO_2$ is kinetically controlled by the mass transfer of CO_2 to the cathode surface, and the increase of j results in more negative working potentials that, at Sn cathodes, were reported to favour hydrogen evolution with respect to CO_2 reduction [6]. The same line of reasoning might be used to rationalize the drop observed for FE_{FA} at 33 mA cm^{-2} for the Ni anode. Rather than mass transfer limitation, which is unlikely because of the high MeOH concentration, in this case the effect is more likely to be related to increased overpotential and, hence, a positive shift of the working potential to values in the region of OER or MeOH oxidation to carbonate [24].

The effect of j was evaluated for the same system by replacing the Ni anode with BDD. As expected, quite similar results were observed in the cathodic compartment (data not shown). Conversely, in the anodic compartment, a quite interesting scenario was observed. Indeed, when j was increased from 11 to 22 and 33 mA cm^{-2}, a corresponding increase of the concentration of FA for the same time passed was observed (figure 9). Specifically, the final [FA] was close to 6, 13 and 20 mM, due to an increase of FE_{FA} as a function of j (figure 9(A)). The final FE_{FA} was 82.0%, 90.0% and 92.5% at 11, 22 and 33 mA cm^{-2}, respectively. Hence, for high j, BDD presented similar or even better FE_{FA} with respect to the Ni anode.

3.6. Effect of charge passed

The experiments discussed in the preceding sections were performed up to a total charge of approximately 200 C. To obtain preliminary insights into the influence of the charge passed on the performance of both the cathodic and anodic pathways, further electrolysis tests were extended to a total charge of 4752 C. These experiments were performed using 0.1 M Na_2SO_4 and 0.5 M NaOH as SEs in the

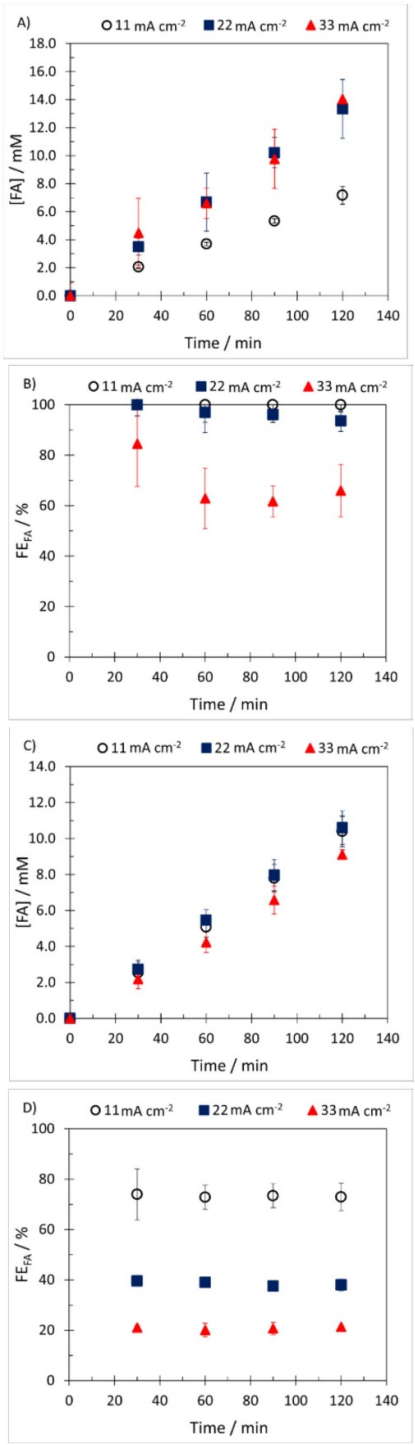


Figure 8. Effect of the current density on [FA] in the anodic (A) and cathodic compartments (C) and on FE_{FA} in the anodic (B) and cathodic compartments (D). The experiments were performed using a Ni NPs anode and a Sn cathode for 2 h in a divided cell with an aqueous solution of 0.1 M Na_2SO_4 in the catholyte and 0.5 M NaOH and 0.5 M CH_3OH in the anolyte.

cathodic and anodic compartments, respectively. Tin cathode and Ni NPs anode, which provided very high FE_{FA} under these operative conditions, were selected as electrodes. In addition, 0.5 M CH_3OH was present in the anolyte.

As shown in figure 10(A), [FA] increases nearly linearly with the charge passed in the cathodic compartment, indicating a good stability of the system over the investigated electrolysis duration. Accordingly, the FE_{FA} at the cathode remained essentially constant at values close to 65%. In the anodic compartment, [FA] increases almost linearly with the charge passed, up to 3000 C with a FE_{FA} close to 100%. Beyond this charge, however, the FE_{FA} at the anode gradually decreased, reaching a final value of 78%. The pH in the anodic compartment exhibited a slow decrease with increasing charge, attaining a

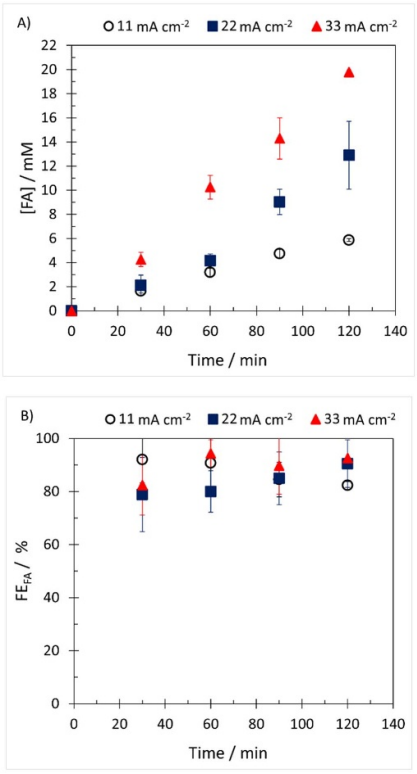


Figure 9. Effect of the current density on the concentration of FA (A) and FE_{FA} (B) in the anodic compartment. Experiments were performed using a BDD anode and a Sn cathode for 2 h in a divided cell with an aqueous solution of 0.1 M Na_2SO_4 in the catholyte and 0.5 M NaOH and 0.5 M CH_3OH in the anolyte.

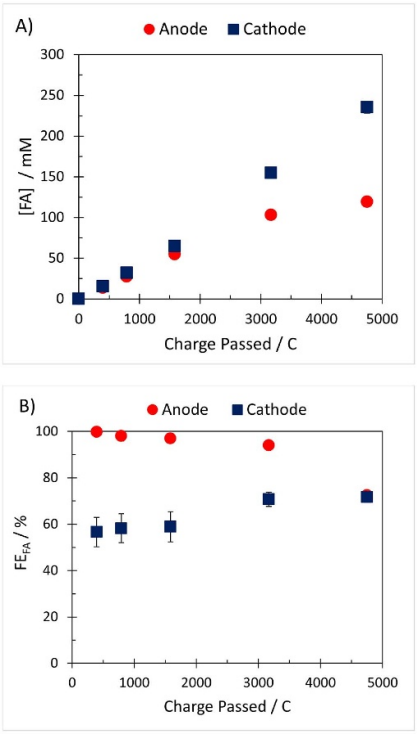


Figure 10. Effect of the charge passed on [FA] (A) and FE_{FA} (B) achieved in the cathodic and anodic compartments. All electrolyses were performed at 22 mA cm^{-2} using a tin cathode and a Ni NPs anode in a divided cell with an aqueous solution of 0.1 M Na_2SO_4 in the catholyte and 0.5 M NaOH + 0.5 M MeOH in the anolyte. $T = 23$ °C.

final value of approximately 12. Therefore, the reduced stability observed at the end of the electrolysis can reasonably be attributed to the gradual pH decrease, although further targeted investigations will be required to fully elucidate the stability limitations.

4. Conclusions

The paired synthesis of formic acid/formate (FA) by cathodic reduction of CO_2 at a Sn cathode and anodic oxidation of MeOH at various anodes was evaluated using aqueous solutions of different electrolytes. It was found that the performance of both cathodic and anodic processes strongly depends on the nature of the electrolyte and on pH even if in opposite ways. Indeed, the presence of high hydroxide ion concentrations, maintaining high pH, favours the anodic conversion of MeOH to FA and limits its oxidation to CO_2. In contrast, high pH is detrimental for the cathodic process as it reduces the availability of key reagents such as CO_2 and H_3O^+. Moreover, it was shown that the performance of MOR strongly depends on the nature of the anode at all adopted SEs. More in detail the most relevant outcome of this study can be summarized as follows.

The cathodic production of FA in NaOH solutions was relatively low at the Sn cathode while the anodic process required alkaline medium and FA production was strongly dependent on the nature of the anode (FE_{FA} increased in the order Ti/IrO_2-Ta_2O_5 < Ti_4O_7 < Cu < Pt < BDD < $Ni(OH)_2$ < Ni NPs). Ni-based electrodes gave very high FE_{FA} in the range 90%–100%, but also BDD gave quite good results with FE_{FA} close to 85%. When $KHCO_3$, which guaranteed an almost neutral pH, was used, the production of FA was higher in the cathodic compartment (FE_{FA} close to 60%) than in NaOH solutions, while FE_{FA} at the anode was significantly lower than in NaOH media and increased in the order Cu < Ti_4O_7 < Ti/RuO_2 < Ti/IrO_2-Ta_2O_5 < Pt < BDD, reaching at maximum of about 20%. The use of Na_2SO_4 aqueous electrolyte allowed to increase the FE_{FA} at the cathode but resulted in low FE_{FA} at the anode (31% at BDD). Hence, diversifying the electrolytes in the anolyte (0.5 M NaOH) and catholyte (0.1 Na_2SO_4) was necessary to achieve quite good FE_{FA} in both compartments.

It was furthermore highlighted that the increase of the current density from 11 to 33 mA cm^{-2} resulted in a considerable decrease FE_{FA} at the cathode, regardless of the anode type. Conversely, opposing effects were observed for MOR at Ni NPs and BDD anodes. FE_{FA} at Ni NPs slightly decreased (from 100% to 94%) upon increasing j from 11 mA cm^{-2} to 22 mA cm^{-2} but dropped to 65% when j = 33 mA cm^{-2} was used. In contrast, FE_{FA} at the BDD anode remained high with an increase from 82% to 92.5% as j was increased from 11 mA cm^{-2} to 33 mA cm^{-2}. Experiments performed for 24 h have shown a good stability for $ERCO_2$ but a small reduction of FE for MOR in the last stages of the tests.

In the future, it will be necessary to evaluate the stability of the system for longer times and to improve the productivity of the cell by studying the potential use of pressurised systems and of gas diffusion cathodes. Also, the potential use of undivided cells will be studied with the aim to avoid the economic penalties given by the use of the membrane.

Acknowledgments

Authors kindly acknowledge financial support from the Italian Ministry of University and Research (MUR) under the PRIN 2022 (Progetti di Rilevante Interesse Nazionale)—Project Code 20229AKSTK, and under the National Recovery Resilience Plan (PNRR) funded by the European Union—NextGenerationEU.

Data availability statement

All data that support the findings of this study are included within the article (and any supplementary files).

Supplementary data available at https://doi.org/10.1088/2515-7655/ae5e0a/data1.

Author contributions

Paola Meli
Data curation (equal), Investigation (equal), Writing – review & editing (equal)

Andrea Antonello
Data curation (equal), Investigation (equal), Methodology (equal)

Andrea Di Franco
Data curation (equal), Investigation (equal)

Alessandro Galia
Project administration (equal), Writing – review & editing (equal)

Lucrezia Greco
Data curation (equal), Investigation (equal)

Abdirisak Ahmed Isse 0000-0003-0966-1983
Conceptualization (equal), Data curation (equal), Methodology (equal), Project administration (equal), Writing – review & editing (equal)

Federica Proietto 0000-0002-9806-7216
Formal analysis (equal), Investigation (equal), Methodology (equal), Writing – review & editing (equal)

Onofrio Scialdone
Conceptualization (equal), Project administration (equal), Supervision (equal), Visualization (equal), Writing – original draft (equal), Writing – review & editing (equal)

References

[1] Bushuyev O S, De Luna P, Dinh C T, Tao L, Saur G, van de Lagemaat J, Kelley S O and Sargent E H 2018 What should we make with CO_2 and how can we make it? *Joule* **2** 825–32
[2] Yaashikaa P R, Senthil Kumar P, Varjani S J and Saravanan A 2019 A review on photochemical, biochemical and electrochemical transformation of CO_2 into value-added products *J. CO2 Util.* **33** 131–47
[3] Jouny M, Luc W and Jiao F 2018 General techno-economic analysis of CO_2 electrolysis systems *Ind. Eng. Chem. Res.* **57** 2165–77
[4] Huang Z *et al* 2021 The economic outlook for converting CO_2 and electrons to molecules *Energy Environ. Sci.* **14** 3664–78
[5] Proietto F, Galia A and Scialdone O 2021 Towards the electrochemical conversion of CO_2 to formic acid at an applicative scale: technical and economic analysis of most promising routes *ChemElectroChem* **8** 2169–79
[6] Proietto F, Patel U, Galia A and Scialdone O 2021 Electrochemical conversion of CO_2 to formic acid using a Sn based electrode: a critical review on the state-of-the-art technologies and their potential *Electrochim. Acta* **389** 138753
[7] Na J *et al* 2019 General technoeconomic analysis for electrochemical coproduction coupling carbon dioxide reduction with organic oxidation *Nat. Commun.* **10** 5193
[8] van den Bosch B *et al* 2022 Research targets for upcycling of CO_2 to formate and carbon monoxide with paired electrolysis *Curr. Opin. Green Sustainable Chem.* **34** 100592
[9] Sabatino S, Galia A, Saracco G and Scialdone O 2017 Development of an electrochemical process for the simultaneous treatment of wastewater and the conversion of carbon dioxide to higher value products *ChemElectroChem* **4** 150–9
[10] Savino U and Sacco A 2021 Tandem devices for simultaneous CO_2 reduction at the cathode and added-value products formation at the anode *J. CO2 Util.* **52** 101697
[11] Verma S, Lu S and Kenis P J A 2019 Co-electrolysis of CO_2 and glycerol as a pathway to carbon chemicals with improved technoeconomics due to low electricity consumption *Nat. Energy* **4** 466–74
[12] Molera M, Fernández-Caso K, Amazian M, Díaz-Sainz G, Solla-Gullón J, Álvarez-Guerra M, Sarret M and Andreu T 2025 Gold–indium electrocatalysts for the selective oxidation of glycerol coupled with CO_2 reduction *ChemSusChem* **18** e202402378
[13] Liu W J, Dang L, Xu Z, Yu H Q, Jin S and Huber G W 2018 Electrochemical oxidation of 5-hydroxymethylfurfural with NiFe layered double hydroxide (LDH) nanosheet catalysts *ACS Catal.* **8** 5533–41
[14] Vass Á, Endrodi B and Janáky C 2021 Coupling electrochemical carbon dioxide conversion with value-added anode processes: an emerging paradigm *Curr. Opin. Electrochem.* **25** 100621
[15] Li M, Wang T, Zhao W, Wang S and Zou Y 2022 A pair-electrosynthesis for formate at ultra-low voltage via coupling of CO_2 reduction and formaldehyde oxidation *Nanomicro Lett.* **14** 211
[16] Lou H, Li N, Zhang R, Chen Y, Xie C, Jiang H, Yang Y and Zhang W 2025 Electrochemical semi-sacrificial growth of Ni-HCP nanoplate arrays for urea/methanol electrooxidation-coupled water electrolysis *Mater. Today Energy* **48** 101779
[17] Lister T E and Dufek E J 2013 Chlor-syngas: coupling of electrochemical technologies for production of commodity chemicals *Energy Fuels* **27** 4244–9
[18] Baessler J *et al* 2024 Reaction engineering for high yield electrosynthesis: unraveling the impact of reaction conditions and conversion on methanol oxidation to formate *Chem. Eng. J.* **495** 153000
[19] Singh M, Sharma H M, Kaur J, Das D K, Ubaidullah M, Gupta R K and Kumar A 2024 Engineering of electrocatalysts for methanol oxidation reaction: recent advances and future challenges *Mol. Catal.* **557** 113982
[20] Hietala J *et al* 2016 Formic Acid *Ullmann's Encyclopedia of Industrial Chemistry* (Wiley) pp 1–22
[21] Bulushev D A and Ross J R H 2018 Towards sustainable production of formic acid *ChemSusChem* **11** 821–36
[22] Wei X, Li Y, Chen L and Shi J 2021 Formic acid electro-synthesis by concurrent cathodic CO_2 reduction and anodic CH_3OH oxidation *Angew. Chem. Int. Ed.* **60** 3148–55

[23] Wu D, Hao J, Song Z, Fu X Z and Luo J L 2021 All roads lead to Rome: an energy-saving integrated electrocatalytic CO_2 reduction system for concurrent value-added formate production *Chem. Eng. J.* **412** 127893
[24] Phan V T T, Nguyen Q P, Wang B and Burgess I J 2024 Oxygen vacancies alter methanol oxidation pathways on NiOOH *J. Am. Chem. Soc.* **146** 4830–41
[25] Feaster J T, Shi C, Cave E R, Hatsukade T, Abram D N, Kuhl K P, Hahn C, Nørskov J K and Jaramillo T F 2017 Understanding selectivity for the electrochemical reduction of carbon dioxide to formic acid and carbon monoxide on metal electrodes *ACS Catal.* **7** 4822–7
[26] Zhao S, Li S, Guo T, Zhang S, Wang J, Wu Y and Chen Y 2019 Advances in Sn-based catalysts for electrochemical CO_2 reduction *Nano-Micro Lett* **11** 62
[27] Yang S Y, Maeng J Y, Hwang S Y, Park G E, Rhee C K and Sohn Y 2023 Electrochemical CO_2 reduction on tin and its alloys: insights from depth-profiling x-ray photoelectron spectroscopy *J. Alloys Compd.* **960** 170903
[28] Whittaker T N, Fishler Y, Clary J M, Brimley P, Holewinski A, Musgrave C B, Farberow C A, Smith W A and Vigil-Fowler D 2024 Insights into electrochemical CO_2 reduction on metallic and oxidized tin using grand-canonical DFT and *In Situ* ATR-SEIRA spectroscopy *ACS Catal.* **14** 8353–65
[29] Elshahawy A M, Ho K H, Hu Y, Fan Z, Hsu Y W B, Guan C, Ke Q and Wang J 2016 Microwave—assisted hydrothermal synthesis of nanocrystal β-$Ni(OH)_2$ for supercapacitor applications *CrystEngComm* **18** 3256–64
[30] Govindan M, Bond A M and Moon I-S 2017 Implementation of concurrent electrolytic generation of two homogeneous mediators under widened potential conditions to facilitate removal of air-pollutants *Sci. Rep.* **7** 29
[31] Wang C-M, Baer D R, Bruemmer S M, Engelhard M H, Bowden M E, Sundararajan J A and Qiang Y 2011 Microstructure of the native oxide layer on Ni and Cr-doped Ni nanoparticles *J. Nanosci. Nanotechnol.* **11** 8488–97
[32] Barakat N A M, Yassin M A, Al-Mubaddel F S and Amen M T 2018 New electrooxidation characteristic for Ni-based electrodes for wide application in methanol fuel cells *Appl. Catal., A* **555** 148–54
[33] Fleischmann M, Korinek K and Pletcher D 1971 The oxidation of organic compounds at a nickel anode in alkaline solution *J. Electroanal. Chem. Interfacial Electrochem.* **31** 39–49
[34] Abdel Rahim M A, Abdel Hameed R M and Khalil M W 2004 Nickel as a catalyst for the electro-oxidation of methanol in alkaline medium *J. Power Sources* **134** 160–9
[35] Gobal F, Valadbeigi Y and Kasmaee L M 2011 On the significance of hydroxide ion in the electro-oxidation of methanol on Ni *J. Electroanal. Chem.* **650** 219–25
[36] Pourbaix M 1966 Atlas of electrochemical equilibria in aqueous solutions *Pergamon*
[37] Hao J, Liu J, Wu D, Chen M, Liang Y, Wang Q, Wang L, Fu X-Z and Luo J-L 2021 In situ facile fabrication of $Ni(OH)_2$ nanosheet arrays for electrocatalytic co-production of formate and hydrogen from methanol in alkaline solution *Appl. Catal., B* **281** 119510
[38] Bender M T, Lam Y C, Hammes-Schiffer S and Choi K-S 2020 Unraveling two pathways for electrochemical alcohol and aldehyde oxidation on NiOOH *J. Am. Chem. Soc.* **142** 21538–47
[39] Qi Y, Zhang Y, Yang L, Zhao Y, Zhu Y, Jiang H and Li C 2022 Insights into the activity of nickel boride/nickel heterostructures for efficient methanol electrooxidation *Nat. Commun.* **13** 4602
[40] Zhu B, Dong B, Wang F, Yang Q, He Y, Zhang C, Jin P and Feng L 2023 Unraveling a bifunctional mechanism for methanol-to-formate electro-oxidation on nickel-based hydroxides *Nat. Commun.* **14** 1686
[41] Wang X *et al* 2020 Materializing efficient methanol oxidation via electron delocalization in nickel hydroxide nanoribbon *Nat. Commun.* **11** 4647
[42] Li J, Yu H, Na J, Jia S, Zhao Y, Lv K, Zhang W, Chi J and Shao Z 2024 Recent advances in selective methanol oxidation electrocatalysts for the co-production of hydrogen and value-added format *Catal. Sci. Technol.* **14** 5525–44
[43] Yuda A, Ashok A and Kumar A 2022 A comprehensive and critical review on recent progress in anode catalyst for methanol oxidation reaction *Catal. Rev.* **64** 126–228
[44] Mekazni D S et al 2022 Why methanol electro-oxidation on platinum in water takes place only in the presence of adsorbed OH *ACS Catal.* **12** 1965–70
[45] Iwasita T 2002 Electrocatalysis of methanol oxidation *Electrochim. Acta* **47** 3663–74
[46] Martínez-Huitle C A, Rodrigo M A, Sirés I and Scialdone O 2015 Single and coupled electrochemical processes and reactors for the abatement of organic water pollutants: a critical review *Chem. Rev.* **115** 13362–407
[47] Hao Y, Ma P, Ma H, Proietto F, Prestigiacomo C, Galia A and Scialdone O 2022 Electrochemical treatment of synthetic wastewaters contaminated by organic pollutants at Ti_4O_7 anode. study of the role of operative parameters by experimental results and theoretical modelling *ChemElectroChem* **9** e202101720
[48] Matsuoka K, Iriyama Y, Abe T, Matsuoka M and Ogumi Z 2005 Alkaline direct alcohol fuel cells using an anion exchange membrane *J. Power Sources* **150** 27–31
[49] Morallón E, Rodes A, Vázquez J L and Pérez J M 1995 Voltammetric and *in-situ* FTIR spectroscopic study of the oxidation of methanol on Pt(hkl) in alkaline media *J. Electroanal. Chem.* **391** 149–57
[50] Scialdone O, Galia A and Randazzo S 2011 Oxidation of carboxylic acids in water at IrO_2–Ta_2O_5 and boron doped diamond anodes *Chem Eng J.* **174** 266–74
[51] Scialdone O, Galia A and Randazzo S 2012 Electrochemical treatment of aqueous solutions containing one or many organic pollutants at boron doped diamond anodes. Theoretical modeling and experimental data *Chem Eng J.* **183** 124–34
[52] Kapałka A, Fóti G and Comninellis C 2007 Investigations of electrochemical oxygen transfer reaction on boron-doped diamond electrodes *Electrochim. Acta* **53** 1954–61
[53] Kapałka A, Lanova B, Baltruschat H, Fóti G and Comninellis C 2009 A DEMS study of methanol and formic acid oxidation on boron-doped diamond electrode *J. Electrochem. Soc.* **156** E149
[54] Scialdone O, Galia A, Lo N G, Proietto F, Sabatino S and Schiavo B 2016 Electrochemical reduction of carbon dioxide to formic acid at a tin cathode in divided and undivided cells: effect of carbon dioxide pressure and other operating parameters *Electrochim. Acta* **199** 332–41
[55] Meli P *et al* 2026 Paired production of formic acid/formate by cathodic reduction of CO_2 at Sn and anodic oxidation of methanol at BDD *Electrochim. Acta* **558** 148491
[56] John J, Wang H, Rus E D and Abruña H D 2012 Mechanistic studies of formate oxidation on platinum in alkaline medium *J. Phys. Chem.* **116** 5810–20
[57] Housmans T H M, Wonders A H and Koper M T M 2006 Structure sensitivity of methanol electrooxidation pathways on platinum: an on-line electrochemical mass spectrometry study *J. Phys. Chem. A* **110** 10021–31